Protoplasma (2019) 256:983–996
https://doi.org/10.1007/s00709-019-01355-5

ORIGINAL ARTICLE

# Comparative analysis of remodelling of the plant–microbe interface in *Pisum sativum* and *Medicago truncatula* symbiotic nodules

Anna V. Tsyganova[1] · Elena V. Seliverstova[1,2] · Nicholas J. Brewin[3] · Viktor E. Tsyganov[1]

Received: 26 October 2018 / Accepted: 7 February 2019 / Published online: 22 February 2019


## Abstract

Infection of host cells by nitrogen-fixing soil bacteria, known as rhizobia, involves the progressive remodelling of the plant–microbe interface. This process was examined by using monoclonal antibodies to study the subcellular localisation of pectins and arabinogalactan proteins (AGPs) in wild-type and ineffective nodules of *Pisum sativum* and *Medicago truncatula.* The highly methylesterified homogalacturonan (HG), detected by monoclonal antibody JIM7, showed a uniform localisation in the cell wall, regardless of the cell type in nodules of *P. sativum* and *M. truncatula*. Low methylesterified HG, recognised by JIM5, was detected mainly in the walls of infection threads in nodules of both species. The galactan side chain of rhamnogalacturonan I (RG-I), recognised by LM5, was present in the nodule meristem in both species and in the infection thread walls in *P. sativum*, but not in *M. truncatula*. The membrane-anchored AGP recognised by JIM1 was observed on the plasma membrane in nodules of *P. sativum* and *M. truncatula*. In *P. sativum*, the AGP epitope recognised by JIM1 was present on mature symbiosome membranes of wild-type nodules, but JIM1 labelling was absent from symbiosome membranes in the mutant Sprint-2Fix$^-$ (*sym31*) with undifferentiated bacteroids, suggesting a possible involvement of AGP in the maturation of symbiosomes. Thus, the common and species-specific traits of cell wall remodelling during nodule differentiation were demonstrated.

**Keywords** Cell wall · Pectin · Arabinogalactan protein · Infection thread · Symbiosome · Defence response

**Abbreviations**

| | |
|---|---|
| MAb | Monoclonal antibody |
| HG | Homogalacturonan |
| RG-I | Rhamnogalacturonan I |
| AGP | Arabinogalactan protein |
| PBS | Phosphate-buffered saline |
| BSA-C | Acetylated bovine serum albumin |
| DAI | Days after inoculation |

Handling Editor: Ulrike Mathesius

**Electronic supplementary material** The online version of this article (https://doi.org/10.1007/s00709-019-01355-5) contains supplementary material, which is available to authorized users.

✉ Viktor E. Tsyganov
tsyganov@arriam.spb.ru

[1] All-Russia Research Institute for Agricultural Microbiology (ARRIAM), Laboratory of Molecular and Cellular Biology, Podbelsky chaussee 3, St.-Petersburg, Russia 196608

[2] Sechenov Institute of Evolutionary Physiology and Biochemistry of the Russian Academy of Sciences, pr. Torez 44, St.-Petersburg, Russia 194223

[3] John Innes Centre, Norwich Research Park, Norwich NR4 7UH, UK

## Introduction

The processes of plant cell growth and plant interaction with microbes are inextricably linked in nature, and the plant cell surface is of great importance in both phenomena (Lionetti et al. 2012; Bellincampi et al. 2014). The cell wall and the underlying plasma membrane play an important role in the growth and differentiation of tissues. Cell walls are composed primarily of polysaccharides which can be subdivided into three major classes: cellulose, pectins, and hemicelluloses (Cosgrove 2005). In addition to polysaccharides, most plant cell walls contain small amounts of structural proteins and glycoproteins such as extensins and arabinogalactan proteins.

During the interaction with rhizobia, the cell walls and extracellular matrix of legumes are part of the intimate interface for developmental coordination and nutrient exchange (Rae et al. 1992; Rich et al. 2014). In incompatible interactions, extracellular matrix can be modified and made more resistant to invasion by the addition of secondary metabolites

such as lignin and suberin (Ivanova et al. 2015), or by the cross-linking of cell wall proteins (Tsyganova et al. 2009a).

Infection of host cells by rhizobia involves the progressive remodelling of the plant–microbial interface. Tissue and cell infection by rhizobia is generally associated with some form of infection thread structure (Brewin 2004). This originates by the invagination of the plasma membrane at the point of penetration of rhizobia into the root hair, and it grows as a result of the synthesis of new wall material. The infection thread is surrounded by a wall continuous with the plant cell wall and with similar polysaccharide composition and grows at its apex as an intrusive tube within the plant cytoplasm. In the lumen of the infection thread, the bacteria are embedded in an amorphous matrix material comprising root nodule AGP-extensins and other plant glycoproteins that are secreted into the lumen. The luminal matrix probably becomes solidified as a result of protein cross-linking by hydrogen peroxide (Brewin 2004).

The cells which contain infection threads and infection droplets can be subdivided into two groups. The first group includes infected cells in which bacteria are released from infection droplets into the host cytoplasm. The second group includes colonised cells in which infection structures (infection threads and infection droplets) have penetrated host cells, but bacterial release did not occur.

To characterise very diverse plant cell wall components, biochemical tools are required that can identify the molecular structures of polysaccharides with high precision. However, this method can only be applied to tissue homogenates from whole organs, and thus it remains unclear which tissue and cell types contain the identified molecules. Monoclonal antibodies (MAbs) developed against cell wall polymers provide an important analytical tool for the study of plant cell wall structure and function at the cellular and tissue level (Bradley et al. 1988; Knox 2008; Ruprecht et al. 2017; Rydahl et al. 2018). Moreover, MAbs have been used to characterise plants carrying mutations in genes associated with cell wall biosynthesis and metabolism. Previous studies have used MAbs that bind epitopes present on homogalacturonan (HG) (Ivanova et al. 2015; Sujkowska-Rybkowska and Borucki 2015; Gavrin et al. 2016), rhamnogalacturonan I (RG-I) (Balestrini et al. 1996; Torode et al. 2018), arabinogalactan protein (AGP), and arabinogalactan protein-extensins (Perotto et al. 1991; Rae et al. 1992; Kardailsky et al. 1996; Tsyganova et al. 2009b) to localise these epitopes in different plant cells and tissues.

In our previous work, we described the distribution of partially methylesterified (unesterified) HG recognised by JIM5 in pea mutants that are ineffective in symbiotic nitrogen fixation (Ivanova et al. 2015). The increase in deposition of unesterified pectin in infection thread walls was observed for mutants SGEFix$^-$-2 (*sym33*) and RisFixV (*sym42*). Unesterified pectin was also found around degrading bacteroids in the mutant RisFixV (*sym42*). The aim of the present study was to analyse the modification and remodelling of the plant cell surface during nodule development. We used monoclonal antibodies to characterise the distribution of the HG, RG-I and AGP in wild-type and ineffective mutant nodules in pea (*Pisum sativum* L.) and barrel medic (*Medicago truncatula* Gaertn.). Surprisingly, we found that the pattern of distribution for RG-I and AGP epitopes in the nodules of *M. truncatula* differs from that in the nodules in *P. sativum*. It seems that the cell wall remodelling during the nodule development has both a conservative and species-specific character.

## Material and methods

### Plant material

*P. sativum* and *M. truncatula* ineffective (Fix$^-$) mutants blocked at different stages of nodule development and corresponding wild types were used (Table 1).

### Bacterial strains, inoculation and plant growth conditions

Seeds were surface-sterilised as described previously (Kitaeva et al. 2016). In all experiments, *P. sativum* plants were inoculated with *Rhizobium leguminosarum* bv. *viciae* strain 3841 (Wang et al. 1982) as described previously (Ivanova et al. 2015). *M. truncatula* plants were inoculated with *Sinorhizobium meliloti* strain 490, constitutively expressing an mCherry fluorescent protein (a derivative of the pHC60 (tetR) plasmid (Cheng and Walker 1998), in which the GFP coding sequence was replaced by the mCherry coding sequence (J. Fournier, LIPM, Toulouse, France, unpublished results) as described previously (Kitaeva et al. 2016). Seeds were planted in plastic pots containing 200 mL of vermiculite and 100 mL nutrient solution without nitrogen (Fåhraeus 1957). Plants were grown in a growth chamber MLR-352H (Sanyo Electric Co., Ltd., Moriguchi, Japan) under controlled conditions: day/night, 16/8 h; temperature, 21 °C; relative humidity 75%; photosynthetic photon flux density of ~ 280 μmol photons $m^{-2}$ $s^{-1}$.

For immunocytochemical analysis, three independent experiments were performed. Nodules of *P. sativum* were harvested at 14 and 28 DAI. Nodules of *M. truncatula* were harvested 13 and 28 DAI for A17 and *dnf1–1*, 11 and 28 DAI for *efd–1*, and 16 and 28 DAI for TR3 (*ipd3*), depending on nodule growth rate of each genotype. For each variant, ten nodules from different plants were analysed.

### Antibodies

Four primary antibodies were used for immunodetection of cell wall antigens (Table 2).

**Table 1** Plant material used in the study

| Lines | Phenotype | References |
|---|---|---|
| *P. sativum* L. | | |
| SGE | Wild-type | Kosterin and Rozov (1993); Tsyganov et al. (1998) |
| SGEFix$^-$-1 (*sym40*)[a] | Hypertrophied infection droplets and infection threads, abnormal bacteroids | Tsyganov et al. (1994); Tsyganov et al. (1998); Voroshilova et al. (2001) |
| SGEFix$^-$-2 (*sym33*)[b] | Abnormal infection thread growth inside nodule, no bacterial release[c] | Tsyganov et al. (1994); Tsyganov et al. (1998); Voroshilova et al. (2001) |
| SGEFix$^-$-3 (*sym26*) | Early senescence | Tsyganov et al. (2000); Serova et al. (2018) |
| Sprint-2 | Wild-type | Borisov et al. (1994) |
| Sprint-2Fix$^-$ (*sym31*) | Undifferentiated bacteroids | Borisov et al. (1994); Borisov et al. (1997) |
| *M. truncatula* Gaertn. | | |
| cv Jemalong A17 | Wild-type | |
| *efd–1* | Hypertrophied infection droplets and infection threads, abnormal bacteroids | Vernié et al. (2008) |
| TR3 (*ipd3*) | Abnormal infection thread growth inside nodule, no bacterial release | Maunoury et al. (2010); Ovchinnikova et al. (2011) |
| *dnf1–1* | Undifferentiated bacteroids | Van de Velde et al. (2010); Wang et al. (2010) |

[a] The *Sym40* gene is orthologous to the *M. truncatula EFD* gene (Nemankin 2011)

[b] The *Sym33* gene is orthologous to the *M. truncatula IPD3* gene (Ovchinnikova et al. 2011)

[c] The mutant line SGEFix$^-$-2 (*sym33*) has leaky phenotype and in some cells or some nodules bacterial release occurs (Tsyganov et al. 1998; Voroshilova et al. 2001)

**Table 2** Primary antibodies used in the study

| Antibody | Dilution FM/IGL | Antigen/epitope | Reference/source |
|---|---|---|---|
| *Pectins* | | | |
| JIM5 | 1:25/1:10; 1:25 | HG domain of pectic polysaccharides, recognises partially methylesterified epitopes of HG, can also bind to unesterified HG | Knox et al. (1990); Verhertbruggen et al. (2009)/www.plantprobes.net |
| JIM7 | 1:25/1:10; 1:25 | HG domain of pectic polysaccharides, recognises partially methylesterified epitopes of HG but does not bind to unesterified HG | Knox et al. (1990); Verhertbruggen et al. (2009)/www.plantprobes.net |
| LM5 | 1:25/1:10; 1:25 | Rhamnogalacturonan-I/linear (1–4)-β-D-galactan with at least three galactose units at non-reducing end | Jones et al. (1997); Andersen et al. (2016)/www.plantprobes.net |
| *Arabinogalactan protein* | | | |
| JIM1 | 1:25/1:25; 1:50 | Plasma membrane arabinogalactan protein/β-linked-galactosyl | Knox and Roberts (1989)/www.plantprobes.net |

*FM* fluorescence microscopy, *IGL* immunogold labelling

## Sample preparation

Nodules were harvested from roots and transferred directly into fixative. Whole nodules were fixed in 2.5% (*v/v*) glutaraldehyde in 0.06 M phosphate buffer, pH 7.2. Nodules were given a glancing cut on one side to allow better penetration of the fixative. After vacuum infiltration, floating nodules were discarded and the fixative was replaced with fresh solution. After overnight incubation at room temperature, nodules were dehydrated in an ethanol series: 30% at 0 °C for 30 min, 50, 70, 90% and 100% at −35 °C for 1 h at each step. For infiltration and polymerisation of *P. sativum* and *M. truncatula* nodules, London Resin White (Polysciences Europe, Eppelheim, Germany) and Lowicryl K4M Resin (Polysciences Europe, Eppelheim, Germany) were used, accordingly. Subsequently, specimens were gradually infiltrated with increasing concentrations of resin in the ratio 1:1, 1:2, 1:3 mixed with ethanol (100%) and finally embedded in corresponding resin using UV polymerisation in a Leica EM AFS2 (Leica Microsystems, Vienna, Austria) at − 20 °C for 48 h in small plastic containers.

## Fluorescence microscopy

For fluorescence microscopy, the embedded material was cut into semi-thin sections (1–2 μm) on a Leica EM UC7 ultramicrotome (Leica Microsystems, Wetzlar, Germany). Sections were placed on glass slides SuperFrost (Menzel-Gläser, Thermo Fisher Scientific, Waltham, MA USA). After blocking of non-specific binding sites by incubating the sections in a blocking solution (5% (*w/v*) bovine serum albumin (BSA), 0.5% (*w/v*) goat serum, 0.05% (*w/v*) cold water fish skin (CWFS)) and following the wash of the slides with 3% BSA (*w/v*) in PBS (2.48 g/L $NaH_2PO_4$, 21.36 g/L $Na_2HPO_4$, 87.66 g/L NaCl, pH 7.2) during 15 min, the sections were incubated with a selected primary MAb diluted (Table 2) in 3% BSA in PBS (pH 7.2) at 37 °C for 1 h. The samples were washed again in 3% BSA in PBS (pH 7.2) two times for 20 min each. The incubation with the secondary goat anti-rat IgG MAb conjugated with Alexa Fluor 488 (Life

Technologies, Grand Island, NY, USA) in 3% BSA in PBS (diluted 1:200) was conducted for 1 h at 37 °C. Then, samples were washed with PBS twice for 20 min each. After a complete drying, sections were covered with a drop of ProLong Gold® antifade reagent (Life Technologies, Grand Island, NY, USA). The sections were examined on a microscope Axio Imager.Z1 (Carl Zeiss, Jena, Germany). Photos were taken using a digital video camera Axiocam 506 (Carl Zeiss, Jena, Germany).

### Transmission electron microscopy

The immunogold labelling was described previously (Tsyganova et al. 2009b; Ivanova et al. 2015). Briefly, for transmission electron microscopy, gold sections, 90–100 nm thick were obtained with a Leica EM UC7 ultramicrotome (Leica Microsystems, Wetzlar, Germany) and collected on formvar-coated gold grids. The grids were placed in PBS for 30 min and 2.50 mM (*w/v*) glycine for 60 min and were blocked in 1% BSA (*w/v*) in PBS for 2 h and then were washed in 0.1% BSA-C in PBS. Sections were incubated with primary antibody diluted (Table 2) in PBS containing 0.1% BSA-C overnight at 4 °C in a moist chamber. The sections were washed five times in PBS containing 0.1% BSA-C and Tween20 and incubated for 2 h in a moist chamber with secondary antibody, rabbit anti-rat conjugated to 10 nm diameter colloidal gold (Amersham International, Little Chalfont, UK), diluted 1:50 in 0.1% BSA-C in PBS. The grids containing sections were washed four times in 0.1% BSA-C in PBS containing Tween20 and twice in water. After washing, sections were counterstained in 2% (*w/v*) aqueous uranyl acetate, followed by lead citrate for 5 min. Ultrathin sections of the selected area were examined using a Tecnai G2 Spirit electron microscope (FEI, Eindhoven, the Netherlands) at 80 kV. Digital micrographs were taken with a MegaView G2 CCD camera (Olympus-SIS, Münster Germany).

### Quantitative analysis of immunogold labelling

For statistical analysis, at least 5 different samples of nodules and at least 20 sectioned walls of infection threads for JIM5 and 100 sectioned symbiosomes for JIM1 were examined. Morphometrical data were obtained as described by Ivanova et al. (2015). Briefly, at least three areas of wall section for each infection thread were evaluated and the number of gold particles per unit area was calculated. The areas and the number of gold particles were measured using software Zen 2 Core version 2.5 (Carl Zeiss, Jena, Germany). The data were presented as the number of gold particle/$\mu m^2$. They were analysed by *t* test using the software SigmaPlot for Windows version 12.5 (Systat Software, Inc., San Jose, California, USA). Means were separated by the Mann-Whitney Rank Sum test ($P \leq 0.001$).

### Controls of the specificity of the immunolabelling

The specificity of the fluorescence and the immunogold labelling procedures was tested by several negative controls. Negative controls were treated either with (i) non-specific secondary antibody (goat anti-mouse IgG) and (ii) gold conjugated secondary antibody (goat anti-rat IgG) without the primary antibody.

Negative controls revealed that no labelling occurred on the sections when they were treated with (i) non-specific secondary antibody (Fig. S1a, c) and (ii) gold-conjugated secondary antibody without the primary antibody (Fig. S1b, d). No specific label was detected, but autofluorescence was observed on both variants of control sections.

## Results

### Immunolocalisation of homogalacturonan epitopes in effective and ineffective nodules of *P. sativum* and *M. truncatula*

The distribution of highly methylesterified HG in nodules of *P. sativum* and *M. truncatula* was studied using MAb JIM7. The JIM7 epitope was predominantly present in the cell walls of infected and uninfected cells and also in the infection thread walls in all analysed genotypes of both species (Fig. 1). A low amount of this epitope was noted also in the cytoplasm and near the vacuole of the infected cells in *M. truncatula* wild-type A17, the mutant lines *efd–1* and TR3 (*ipd3*) (Fig. 1a–c respectively) and in *P. sativum* mutant line SGEFix$^-$-1 (*sym40*) (Fig. 1f). Immunogold localisation of JIM7 epitope showed that highly methylesterified HG was distributed evenly in cell walls and infection thread walls in small quantities in all genotypes analysed (Fig. 2a, b, d, f). In *P. sativum* mutant line SGEFix$^-$-1 (*sym40*), gold particles of JIM7 were observed near the sites of bacterial release (Fig. 2c). In *M. truncatula* mutant TR3 (*ipd3*), JIM7 labelling was detected in the amorphous material near the infection thread wall (Fig. 2e).

Immunolocalisation of the low methylesterified (unesterified) HG epitope labelled by MAb JIM5 showed that JIM5 epitope was present mostly in the infection thread walls and in cell walls in the sites of the cell junctions in symbiotic nodules of *M. truncatula* (Fig. 3a–d). Immunogold localisation did not reveal any significant differences in the distribution of unesterified HG epitope in the infection thread walls between analysed genotypes (Fig. 4). However, the quantitative analysis showed that the pectic epitope recognised by MAb JIM5 was increased with nodule ageing in all genotypes except *efd–1* (Table 3) and the amount of label was significantly higher in wild-type nodules in comparison with mutant nodules, except for 28-day-old nodules of the mutant TR3 (*ipd3*) (Table 3).

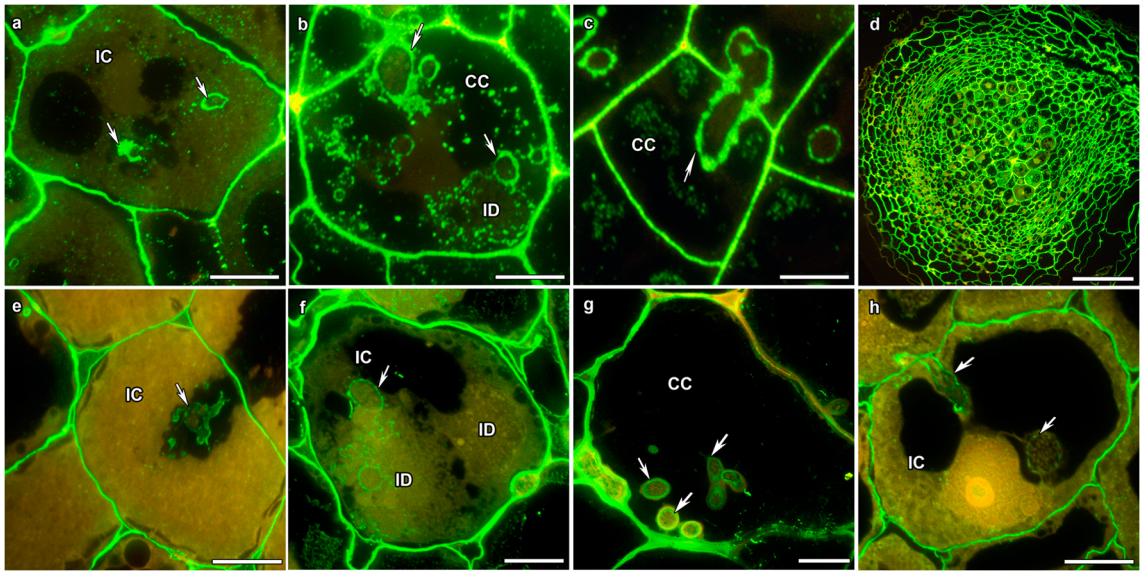


**Fig. 1** Fluorescent immunolocalisation of highly methylesterified homogalacturonan epitope labelled with JIM7 in nodules from wild-type and mutant lines of *M. truncatula* (**a**–**d**) and *P. sativum* (**e**–**h**). The secondary antibody used was goat anti-rat IgG MAb conjugated with Alexa Fluor 488. IC infected cell, CC colonised cell, ID infection droplet; arrows indicate infection threads. **a** Wild-type A17, 13 DAI. **b** Mutant *efd–1*, 11 DAI. **c** Mutant TR3 (*ipd3*), 16 DAI. **d** Mutant *dnf1–1*, 13 DAI. **e** Wild-type SGE, 14 DAI. **f** Mutant SGEFix$^-$-1 (*sym40*), 14 DAI. **g** Mutant SGEFix$^-$-2 (*sym33*), 14 DAI. **h** Mutant Sprint-2Fix$^-$ (*sym31*), 14 DAI. *Bar* = 20 μm (**a**, **e**–**h**), *bar* = 10 μm (**b**, **c**), *bar* = 200 μm (**d**)

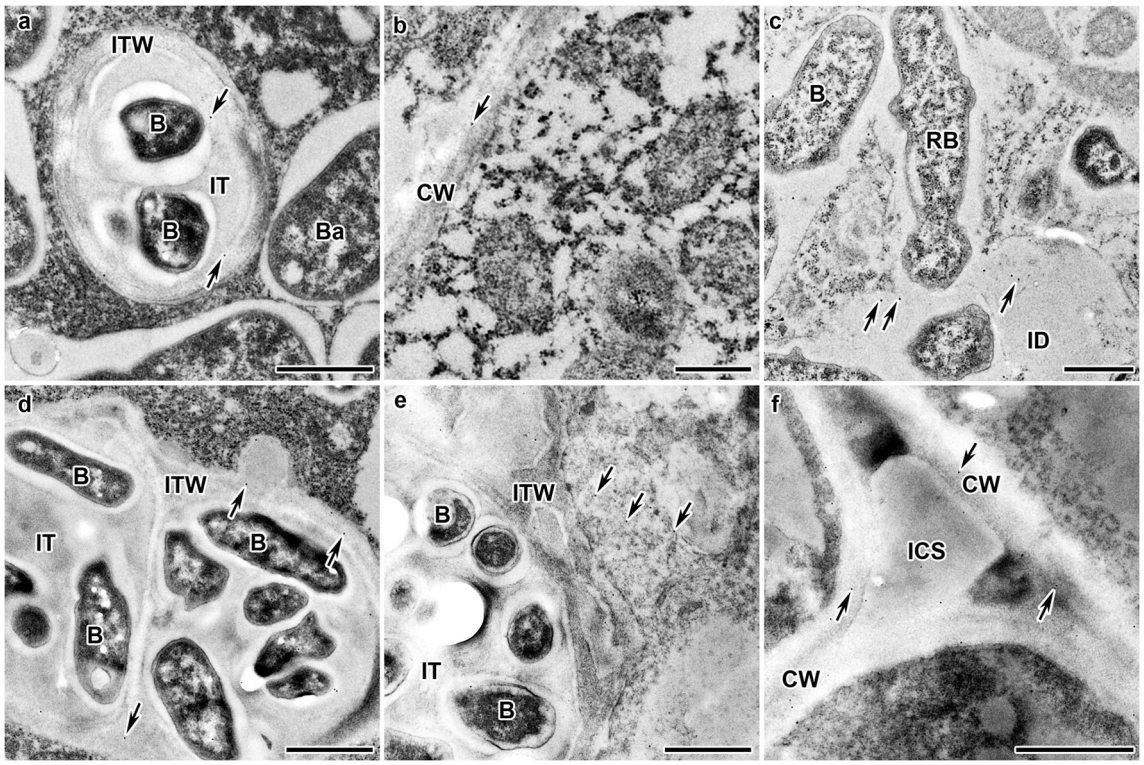


**Fig. 2** Immunogold localisation of highly methylesterified homogalacturonan epitope labelled with JIM7 in the nodules of wild-type and mutant lines from *P. sativum* (**a**–**d**) and *M. truncatula* (**e**, **f**). The secondary antibody used was goat anti-rat IgG MAb conjugated to 10 nm diameter colloidal gold. IT infection thread, ITW infection thread wall, ID infection droplet, CW cell wall, ICS intercellular space, B bacterium, RB releasing bacterium, Ba bacteroid; arrows indicate gold particles. **a** Wild-type SGE, 14 DAI. **b** Wild-type SGE, 28 DAI. **c** Mutant SGEFix$^-$-1 (*sym40*), 14 DAI. **d** Mutant SGEFix$^-$-2 (*sym33*), 14 DAI. **e** Mutant TR3 (*ipd3*), 28 DAI. **f** Mutant *dnf1–1*, 13 DAI. *Bar* = 500 nm (**a**, **c**–**f**); *bar* = 200 nm (**b**)

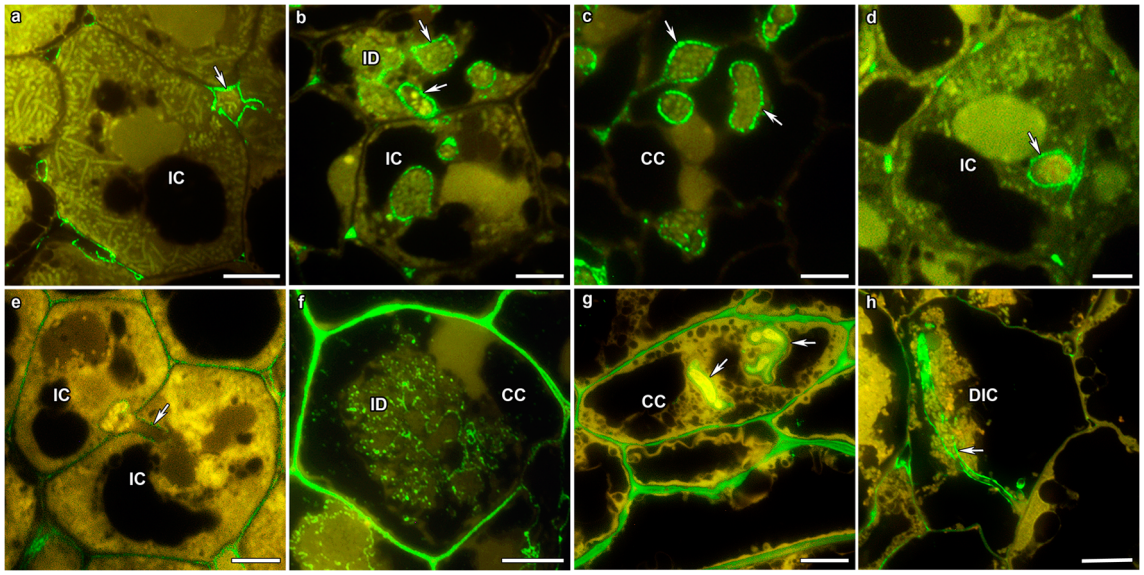


**Fig. 3** Fluorescent immunolocalisation of low methylesterified (unesterified) homogalacturonan epitope labelled with JIM5 in nodules from wild-type and mutant lines of *M. truncatula* (**a**–**d**) and *P. sativum* (**e**–**h**). The secondary antibody used was goat anti-rat IgG MAb conjugated with Alexa Fluor 488. IC infected cell, CC colonised cell, DIC degrading infected cell, ID infection droplet; arrows indicate infection threads. **a** Wild-type A17, 13 DAI. **b** Mutant *efd–1*, 11 DAI. **c** Mutant TR3 (*ipd3*), 16 DAI. **d** Mutant *dnf1–1*, 13 DAI. **e** Wild-type SGE, 14 DAI. **f** Mutant SGEFix$^{-}$-1 (*sym40*), 14 DAI. **g** Mutant SGEFix$^{-}$-2 (*sym33*), 14 DAI. **h** Mutant SGEFix$^{-}$-3 (*sym26*), 14 DAI. *Bar* = 20 μm (**a**, **e**–**h**), *bar* = 10 μm (**c**, **d**)

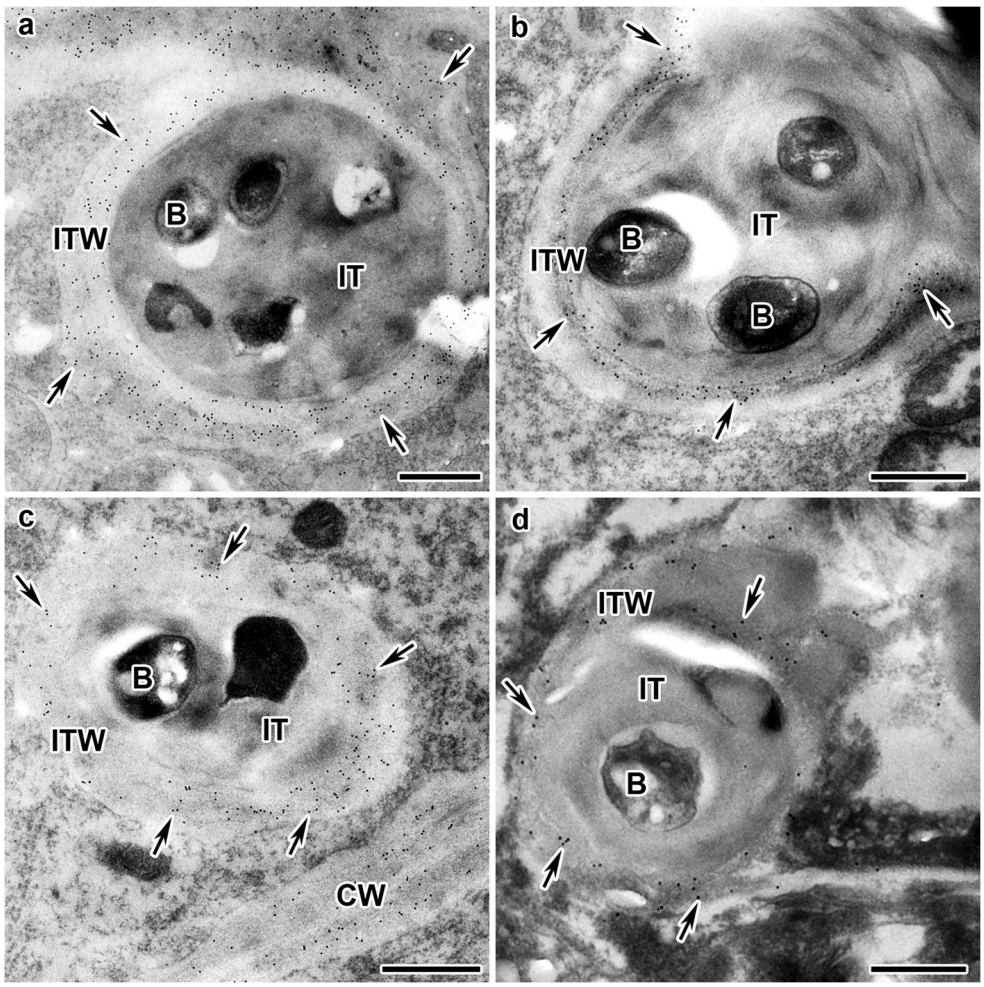


**Fig. 4** Immunogold localisation of low methylesterified (unesterified) homogalacturonan epitope labelled with JIM5 in the nodules of *M. truncatula* wild-type and mutant lines. The secondary antibody used was goat anti-rat IgG MAb conjugated to 10 nm diameter colloidal gold. IT infection thread, ITW infection thread wall, CW cell wall, B bacterium; arrows indicate gold particles. **a** Wild-type A17, 13 DAI. **b** Mutant *efd–1*, 11 DAI. **c** Mutant TR3 (*ipd3*), 16 DAI. **d** Mutant *dnf1–1*, 13 DAI. *Bar* = 500 nm

**Table 3** Distribution of unesterified HG epitope labelled with JIM5 in infection thread walls in wild-type and mutant lines of *M. truncatula*

| Genotypes | Days after inoculation (DAI) | Mean value | SE |
|---|---|---|---|
| cv Jemalong A17 (wt) | 13 | 68.4[c] | 4.3 |
| | 28 | 84.4 | 2.7 |
| *efd–1* | 11 | 57.1[a] | 3.1 |
| | 28 | 59.3[b] | 2.3 |
| TR3 (*ipd3*) | 16 | 47.2[ac] | 3.5 |
| | 28 | 94.8[b] | 4.0 |
| *dnf1–1* | 13 | 34.5[ac] | 2.7 |
| | 28 | 64.6[b] | 4.2 |

Results are presented as the number of gold particles/μm$^2$ . Mean value ± SE ($n = 20–25$) are shown. Letters indicate statistically significant differences (*t* test, *P* value ≤ 0.001)

[a] From the wild-type A17 of corresponding mutant lines at 2 WAI

[b] From the wild-type A17 of corresponding mutant lines at 4 WAI

[c] Within genotype compared with 4 WAI

Fluorescence microscopy showed that in *P. sativum*, the JIM5 epitope was detected in cell walls and infection thread walls in all genotypes investigated (Fig. 3e–h) but in mutants SGEFix$^-$-1 (*sym40*) (Fig. 3f) and SGEFix$^-$-2 (*sym33*) (Fig. 3g), the JIM5 label was more abundant in cell walls. Previously, we have demonstrated that the amount of JIM5 label in infection thread walls was highly increased in SGEFix$^-$-2 (*sym33*) nodules (Ivanova et al. 2015). In this study, quantitative analysis of JIM5 label revealed a slight decrease in its amount in SGEFix$^-$-3 (*sym26*) and Sprint-2Fix$^-$ (*sym31*) in comparison with SGE and Sprint-2 (Table 4).

**Table 4** Distribution of unesterified HG epitope labelled with JIM5 in infection thread walls in wild-type and mutant lines of *P. sativum* L. at 14 days after inoculation (DAI)[c]

| Genotypes | Mean value | SE |
|---|---|---|
| SGE (wt) | 123 | 6.5 |
| SGEFix$^-$-3 (*sym26*) | 93[a] | 8.1 |
| Sprint-2 (wt) | 112 | 8.6 |
| Sprint-2Fix$^-$ (*sym31*) | 103[b] | 8.3 |

Mean value ± SE ($n = 20–25$) are shown. Letters indicate statistically significant differences (*t* test, *P* value ≤ 0.001). Results are presented as the number of gold particles/μm$^2$

[a] From the wild-type SGE of corresponding mutant line at 14 DAI

[b] From the wild-type Sprint-2 of corresponding mutant line at 14 DAI

[c] Data for mutants SGEFix$^-$ -1 (*sym40*) and SGEFix$^-$ -2 (*sym33*) in the table are not presented, since they coincide with those presented previously (Ivanova et al. 2015)

## Immunolocalisation of rhamnogalacturonan-I epitope in effective and ineffective nodules of *P. sativum* and *M. truncatula*

Fluorescent microscopy of the linear (1–4)-β-D-galactan epitope of RG-I recognised by the MAb LM5 showed that, in symbiotic nodules of *M. truncatula*, labelling was observed only in meristematic cell walls in wild-type A17 (Fig. S2a) and corresponding mutants (data not shown) at both the dates of analysis. In nodules of *P. sativum*, LM5 labelling was defined in walls of meristematic (data not shown), endodermis and phloem cells and also in infection thread walls in all genotypes analysed (Fig. S2 and Fig. 5). LM5 epitope was also present in the sites of the junctions of uninfected cells in the mutant line SGEFix$^-$-2 (*sym33*) (Fig. S2b). The high intensity of fluorescence labelling by LM5 was detected in the cell wall of the nodule endodermis (Fig. S2c) and vascular bundles (Fig. S2d). In infected cells of *P. sativum* wild-type SGE (Fig. 5a) and mutant line Sprint-2Fix$^-$ (*sym31*) nodules (Fig. 5f), the intense signal of LM5 epitope labelling was observed mainly in the infection thread walls. The LM5 label was also observed in infection thread walls in colonised cells of the mutants SGEFix$^-$-1 (*sym40*) (Fig. 5b) and SGEFix$^-$-2 (*sym33*) (Fig. 5c). However, it was absent in some infection thread walls in mutant line SGEFix$^-$-2 (*sym33*) (Fig. 5d). In the mutant line SGEFix$^-$-3 (*sym26*), which has an early senescence phenotype (Serova et al. 2018), LM5 epitope was observed in the cell wall of senescent uninfected cells (Fig. 5e). Immunogold analysis confirmed the localisation of the LM5 antibody in infection thread walls of wild types and mutant pea lines (Fig. 6). The linear (1–4)-β-D-galactan epitope of RG-I recognised by the MAb LM5 was not detected in any of the colonised or infected cells in symbiotic nodules of *M. truncatula*, independent of the genotype.

## Immunolocalisation of arabinogalactan protein epitope in effective and ineffective nodule of *P. sativum* and *M. truncatula*

The AGP epitope recognised by the MAb JIM1 was present in a very low amount in the plasma membrane of the infected cells of *M. truncatula* (Fig. 7a and Fig. S3). In 14-day-old nodules of *P. sativum* wild-type SGE, the JIM1 label was observed in the symbiosome and plasma membranes of the infected cells (Fig. 7b). In 28-day-old nodules, the intensity of the fluorescent signal associated with the symbiosome membrane was significantly increased (Fig. 7c). In 14-day-old nodules of mutant line SGEFix$^-$-1 (*sym40*), characterised with abnormal bacteroids (Tsyganov et al. 1998), the level of JIM1 labelling

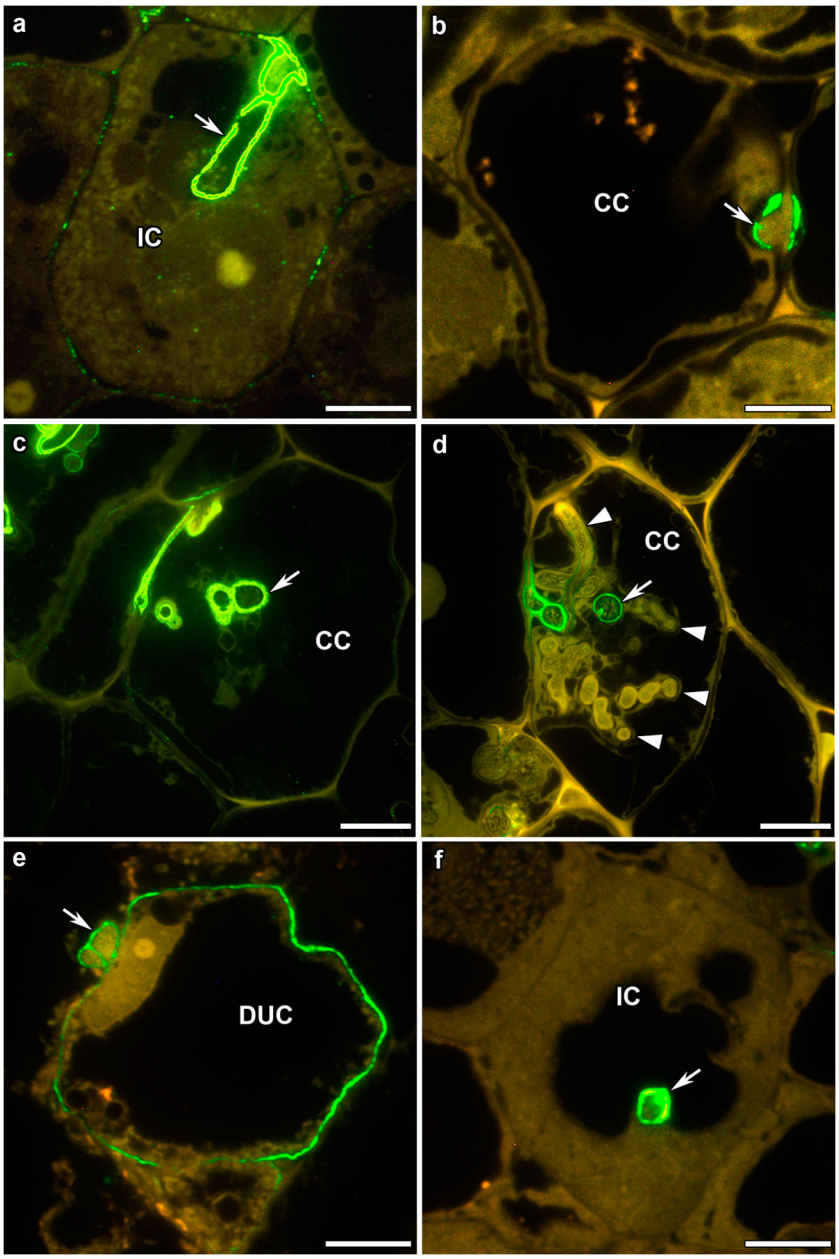


**Fig. 5** Fluorescent immunolocalisation of rhamnogalacturonan I epitope labelled with LM5 in the 14-day-old nodules of *P. sativum* wild-type and mutant lines. The secondary antibody used was goat anti-rat IgG MAb conjugated with Alexa Fluor 488. IC infected cell, CC colonised cell, DUC degrading uninfected cell; arrows indicate infection threads with labelling, arrowheads—infection threads without labelling. **a** Wild-type SGE. **b** Mutant SGEFix$^-$-1 (*sym40*). **c**, **d** Mutant SGEFix$^-$-2 (*sym33*). **e** Mutant SGEFix$^-$-3 (*sym26*). **f** Mutant Sprint-2Fix$^-$ (*sym31*). *Bar* = 20 μm

was similar to that in wild-type SGE (Fig. 7e). In 14-day-old nodules of mutant line SGEFix$^-$-3 (*sym26*), characterised with premature degradation of symbiotic structures (Serova et al. 2018), the intensity of fluorescent signal was similar to the intensity of the signal in 28-day-old nodules of the wild-type (Fig. 7f). However, in nodules of the mutant lines Sprint-2Fix$^-$ (*sym31*) characterised by the presence of undifferentiated bacteroids (Borisov et al. 1997), the intensity of JIM1 signal was weak in the symbiosome membranes (Fig. 7d).

With respect to the AGP epitope recognised by the MAb JIM1, gold particle decoration was principally found in the symbiosome membrane and peribacteroid space, although some labelling was also observed in the plasma membrane (Fig. 8). Immunogold localisation confirmed the increased JIM1 labelling in the symbiosomes of *P. sativum* wild types SGE (Fig. 8e) and Sprint-2 in 28-day-old nodules (Table 5). In 14-day-old nodules of the mutant line SGEFix$^-$-2 (*sym33*) (in cells where bacterial release occurred) (Fig. 8c) and the mutant line SGEFix$^-$-3 (*sym26*) (Fig. 8g), the symbiosome membranes were extensively labelled by JIM1 in comparison with wild-type SGE (Table 5). In nodules of the mutant line SGEFix$^-$-1 (*sym40*), the JIM1 label was present in a very low amount (Table 5) in both symbiosomes containing several bacteroids (Fig. 8b) or a single bacteroid (Fig. 8f). In 14- and 28-day-old nodules of the mutant line Sprint-2Fix$^-$ (*sym31*) gold particles of the JIM1 label were observed only rarely in the symbiosome membrane (Fig. 8h; Table 5).

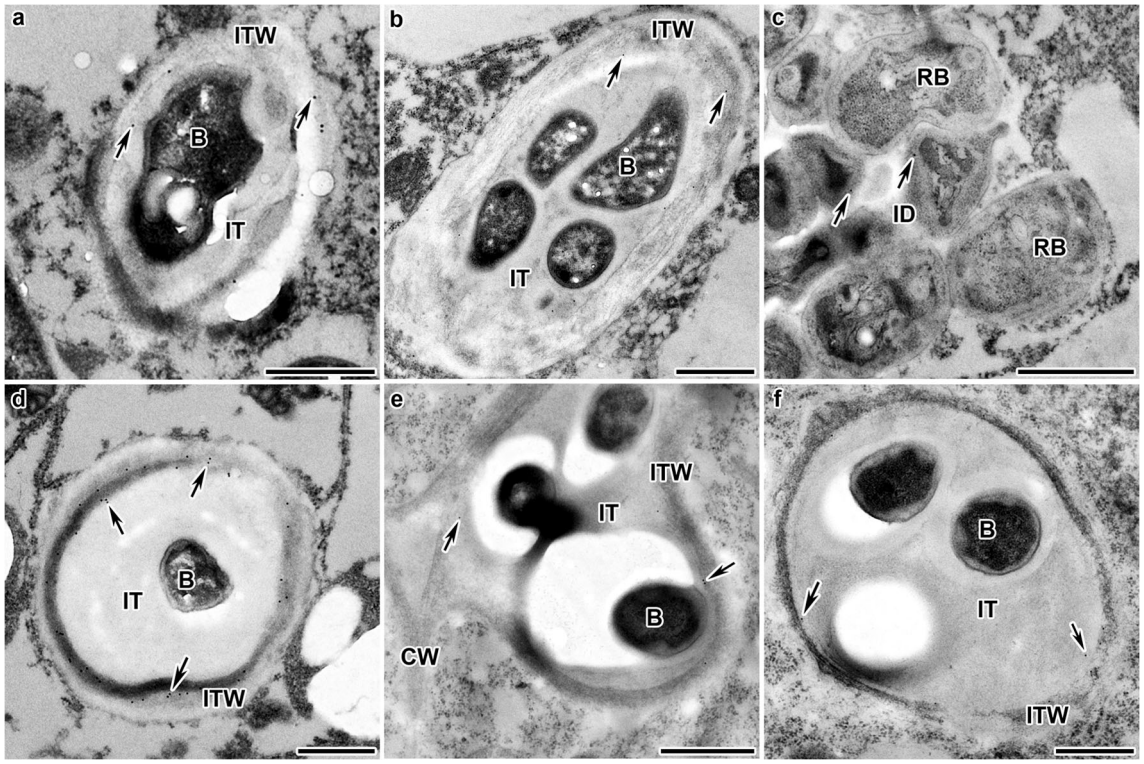


**Fig. 6** Immunogold localisation of rhamnogalacturonan I epitope labelled with LM5 in the infection threads from nodules of *P. sativum* wild-type and mutant lines. The secondary antibody used was goat anti-rat IgG MAb conjugated to 10 nm diameter colloidal gold. IT infection thread, ID infection droplet, ITW infection thread wall, CW cell wall, B bacterium, RB released bacterium; arrows indicate gold particles. **a** Wild-type SGE, 14 DAI. **b** Mutant SGEFix$^-$-1 (*sym40*), 14 DAI. **c** Mutant SGEFix$^-$-1 (*sym40*), 28 DAI. **d** Mutant SGEFix$^-$-2 (*sym33*), 14 DAI. **e** Mutant Sprint-2Fix$^-$ (*sym31*), 14 DAI. **f** Mutant SGEFix$^-$-3 (*sym26*), 14 DAI. *Bar* = 500 nm

## Discussion

Pectins constitute one of the main components of the plant cell wall. They are a family of galacturonic acid-rich polysaccharides including homogalacturonan (HG), rhamnogalacturonan I and the substituted galacturonans, rhamnogalacturonan II and xylogalacturonan (Caffall and Mohnen 2009). Methylesterification of HG is tightly regulated by the plant and pectic polysaccharides are deposited in a tissue-specific and spatiotemporal manner (Anderson 2015; Levesque-Tremblay et al. 2015). Studies using antibodies against highly methylesterified HG (JIM7 and LM20) or HG with a lower degree of methylesterification (JIM5 and LM19) have shown that the distribution of HGs with different levels of methylesterification can vary on a very small spatial scale within tissues, indicating an important role in cell development (Gawecki et al. 2017; Liu et al. 2017; Sala et al. 2017).

During nodule development in *P. sativum*, uniform labelling with JIM7, which recognises highly methylesterified pectin, has previously been demonstrated throughout both the cell wall and the infection thread wall (Rae et al. 1992). This observation was confirmed in our own studies for both *P. sativum* and *M. truncatula* (Fig. 1), indicating a uniform cell wall structure in which the pectin matrix does not show any sign of localised loosening or stiffening. In nodules of *P. sativum*, binding of JIM5, which recognises low methylesterified pectin, was localised to the middle lamella of the cell walls and was predominantly on the luminal side of the infection thread wall (Rae et al. 1992). Similarly in the present study, low methylesterified HG labelled by JIM5 was detected mainly in the infection thread walls of wild-type symbiotic nodules of both *P. sativum* and *M. truncatula*.

Previously, we demonstrated an increase in deposition of unesterified pectin in infection thread walls of the *P. sativum* mutant lines SGEFix$^-$-2 (*sym33*) and RisFixV (*sym42*) (Ivanova et al. 2015). By contrast, in the pea mutant lines without abnormalities in infection thread development, SGEFix$^-$-3 (*sym26*) and Sprint-2Fix$^-$ (*sym31*), the distribution of unesterified HGs did not differ from wild-type and the level of JIM5 labelling was slightly decreased compared to corresponding wild types (Table 4). Surprisingly, in nodules of SGEFix$^-$-2 (*sym33*) (Fig. 3g) and especially SGEFix$^-$-1 (*sym40*) (Fig. 3f), the intensity of JIM5 label was high in the walls of colonised cells. Possibly, this pattern of distribution for low methylesterified HG might be caused by activation of a cellular defence response in these mutants (Ivanova et al. 2015). It has previously been reported that methyl esterification of pectin plays a role during plant–pathogen interactions and affects plant resistance to diseases (Lionetti et al. 2012).

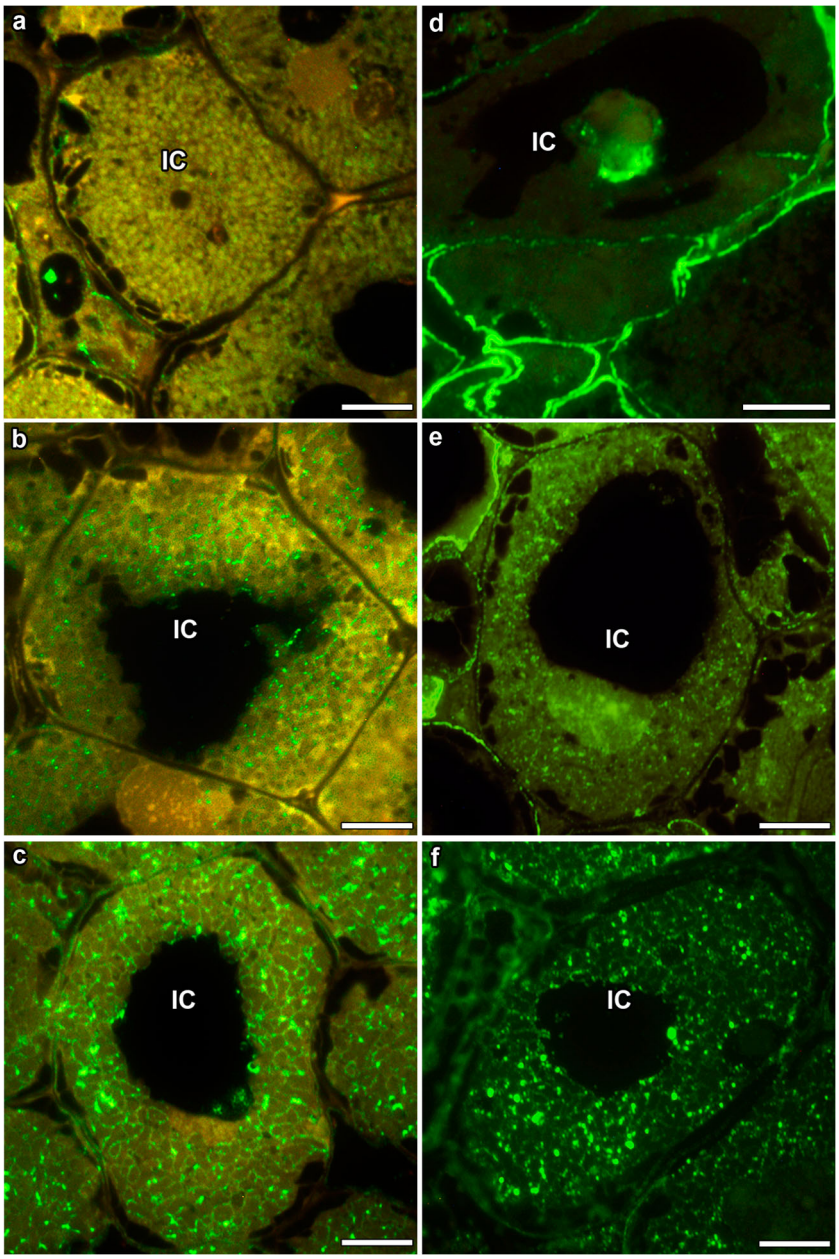


**Fig. 7** Fluorescent immunolocalisation of arabinogalactan protein epitope labelled with JIM1 in the nodules of the *M. truncatula* (**a**) and *P. sativum* (**b**–**f**) wild types and mutant lines. The secondary antibody used was goat anti-rat IgG MAb conjugated with Alexa Fluor 488. IC infected cell. **a** Wild-type A17, 13 DAI. **b** Wild-type SGE, 14 DAI. **c** Wild-type SGE, 28 DAI. **d** Mutant Sprint-2Fix$^-$ (*sym31*), 14 DAI. **e** Mutant SGEFix$^-$-1 (*sym40*), 14 DAI. **f** Mutant SGEFix$^-$-3 (*sym26*), 14 DAI. *Bar* = 20 μm

In *M. truncatula* nodules, we observed a somewhat similar distribution pattern for the low methylesterified HG in infection threads (Table 3). In all mutant genotypes analysed at the first date, the amount of JIM5 label was lower than in wild-type. However, in 28-day-old nodules in the mutant line TR3 (*ipd3*) (*IPD3* is orthologous to *Sym33* (Ovchinnikova et al. 2011)), the abundance of JIM5 gold particles was higher than in wild-type. In nodules of SGEFix$^-$-2 (*sym33*), the increase in JIM5 label was more pronounced and was already evident in infection thread walls from 14-day-old nodules (Ivanova et al. 2015). It is interesting to note that a doubling of the amount of label for de-esterified HG was also observed in the *M. truncatula* mutant line *dnf1–1*, which is characterised by undifferentiated bacteroids (Van de Velde et al. 2010) (Table 3).

Another cell wall component with tissue-specific variation is rhamnogalacturonan I (RG-I). With a variety of molecular structures, RG-I is usually considered to be a component of thin primary cell walls, where it acts as a "glue" to keep neighbouring cells together (Gorshkova et al. 2013). It is a hypervariable pectic polysaccharide with substitution by a complex array of side chains in which (1–4)-β-D-galactan and (1–5)-α-L-arabinan often predominate (Torode et al. 2018). RG-I has been implicated in the modification of mechanical properties such as cell wall firmness and cell wall elasticity (Saffer 2018; Torode et al. 2018).

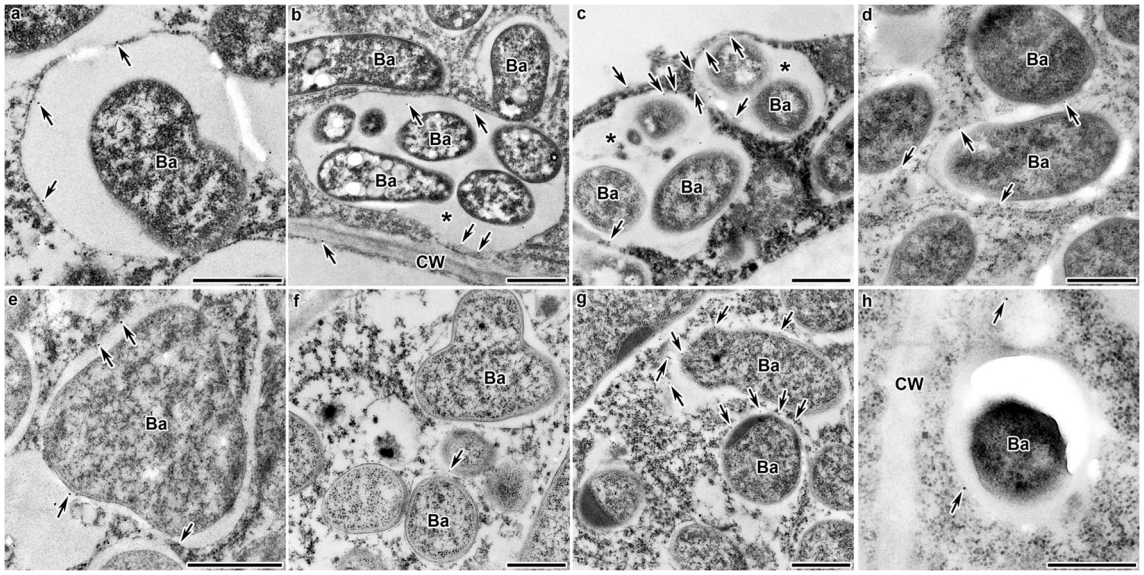


**Fig. 8** Immunogold localisation of arabinogalactan protein epitope labelled with JIM1 in the nodules of the *P. sativum* wild-type and mutant lines. The secondary antibody used was goat anti-rat IgG MAb conjugated to 10 nm diameter colloidal gold. CW cell wall, Ba bacteroid; *several bacteroids surrounded by a common symbiosome membrane; arrows indicate gold particles. **a** Wild-type SGE, 14 DAI. **b** Mutant SGEFix$^-$-1 (*sym40*), 14 DAI. **c** Mutant SGEFix$^-$-2 (*sym33*), 14 DAI. **d** Wild-type Sprint-2, 14 DAI. **e** Wild-type SGE, 28 DAI. **f** Mutant SGEFix$^-$-1 (*sym40*), 28 DAI. **g** Mutant SGEFix$^-$-3 (*sym26*), 14 DAI. **h** Mutant Sprint-2Fix$^-$ (*sym31*), 14 DAI. *Bar* = 500 nm

Arabinan and galactan side chains of RG-I frequently have distinct or mutually exclusive patterns of localisation. In general, arabinan tends to be predominant in younger cells, while expanding cells tend to have more galactan (Willats et al. 1999; Herbette et al. 2014; Corral-Martínez et al. 2016; Liu et al. 2017). In contrast to these observations, the galactan side chain of RG-I recognised by LM5 was present in the meristematic cells in the nodules of both species (Fig. S2). However, in the mature nodule, the epitope was restricted to the cells of the nodule endodermis (Fig. S2c) and in sieve elements of the vascular bundles (Fig. S2d).

**Table 5** Distribution of AGP epitope recognised by the MAb JIM1 in symbiosomes of infected cells in pea wild-type and mutant lines

| Genotypes | Days after inoculation (DAI) | Mean value | SE |
|---|---|---|---|
| SGE (wt) | 14 | 4.10$^{e}$ | 0.40 |
| | 28 | 6.13 | 0.71 |
| SGEFix$^-$-1 (*sym40*) | 14 | 3.28$^{ae}$ | 0.35 |
| | 28 | 1.09$^{b}$ | 0.25 |
| SGEFix$^-$-2 (*sym33*) | 14 | 7.38$^{ae}$ | 0.79 |
| | 28 | 4.65$^{b}$ | 0.49 |
| SGEFix$^-$-3 (*sym26*) | 14 | 11.46$^{ae}$ | 0.66 |
| | 28 | 2.04$^{b}$ | 0.33 |
| Sprint-2 (wt) | 14 | 4.50$^{e}$ | 0.46 |
| | 28 | 6.54 | 0.52 |
| Sprint-2Fix$^-$ (*sym31*) | 14 | 1.07$^{c}$ | 0.35 |
| | 28 | 1.11$^{d}$ | 0.26 |

Results are presented as the number of gold particles/μm$^2$ . Mean value ± SE ($n$ = 100–150) are shown. Letters indicate statistically significant differences ($t$ test, $P$ value ≤ 0.001)

[a] From the wild-type SGE of corresponding mutant lines at 14 DAI

[b] From the wild-type SGE of corresponding mutant lines at 28 DAI

[c] From the wild-type Sprint-2 of corresponding mutant line at 14 DAI

[d] From the wild-type Sprint-2 of corresponding mutant line at 28 DAI

[e] Within genotype compared with 28 DAI

In *P. sativum* nodules, the infection thread walls were labelled with LM5 antibody which recognises the galactan side chain of RG-I (Figs. 5 and 6). However, in *M. truncatula*, LM5 did not label infection thread walls. This may indicate slight differences in the composition of the infection thread wall in *P. sativum* and *M. truncatula*. The pattern of LM5 labelling was basically similar in *P. sativum* wild-type and mutant nodules; although, in the nodules of mutant line SGEFix$^-$-2 (*sym33*), we found that some infection thread walls were not labelled by LM5 (Fig. 5d). Furthermore, in nodules in the mutant line SGEFix$^-$-3 (*sym26*) characterised with premature degradation of symbiotic structures (Serova et al. 2018), the galactan side chain of RG-I accumulated in the cell wall of uninfected cells in the senescent zone (Fig. 5e). The biological significance of this accumulation is still unclear.

Arabinogalactan proteins (AGPs) are one of the most complex families of macromolecules found in plants. They have been implicated in many processes involved in plant growth and development (Showalter 2001; Ellis et al. 2010), but their precise mode of action is unknown (Brewin 2004; Nguema-Ona et al. 2013; Saffer 2018). The possibility that AGPs can be anchored to the plasma membrane via a glycosylphosphatidylinositol (GPI) anchor indicates a possible role in cell wall remodelling during the establishment of the symbiotic interface (Sherrier et al. 1999). In

the present study, it was observed that the membrane-anchored AGP recognised by JIM1 was present not only on the plasma membrane of *P. sativum* nodules, but also on the symbiosome membrane (Fig. 7). The increase in JIM1 labelling in symbiosomes in 28-day-old nodules compared to 14-day-old nodules suggests that AGP recognised by JIM1 participates in the maturation of symbiosomes in wild-type nodules of *P. sativum* (Fig. 7a, b; Table 5).

The mutant line Sprint-2Fix$^-$ (*sym31*), characterised by undifferentiated bacteroids (Borisov et al. 1997), displayed preferential localisation of AGP (JIM1-epitope) on the plasma membrane (Fig. 7d) and a constant low level in symbiosomes, confirming the reduced level of differentiation for the symbiosome membrane in this mutant (Table 5). The developmental progression of symbiosomes of mutant Sprint-2Fix$^-$ (*sym31*) was previously studied by using the antibody JIM18 which recognised a glycolipid component of the plasma membrane and juvenile symbiosomes (Sherrier et al. 1997). In the mutant Sprint-2Fix$^-$ (*sym31*), labelling with JIM18 was uniform throughout the infected cells of the nodule, confirming that only the juvenile form of symbiosome membrane was present in the mutant Sprint-2Fix$^-$ (*sym31*) nodules (Sherrier et al. 1997; Dahiya et al. 1998).

The mutant line SGEFix$^-$-3 (*sym26*), with an early senescence phenotype, displayed a significantly higher amount of JIM1 label in 14-day-old nodules than in wild-type nodules (Table 5). In 28-day-old nodules, the amount of JIM1 label was abruptly decreased, in contrast to wild-type nodules (Table 5). A similar pattern was observed in another mutant line, SGEFix$^-$-2 (*sym33*), which was characterised by occasional bacterial release in some cells of some nodules (Voroshilova et al. 2001). In the mutant line SGEFix$^-$-1 (*sym40*), forming nodules with bacteroids of abnormal shape (Tsyganov et al. 1998), the amount of JIM1 label was also decreased in 28-day-old nodules compared to 14-day-old ones, but it did not differ in 14-day-old mutant nodules compared to wild-type 14-day-old nodules (Table 5). The observed differences in JIM1-epitope accumulation in nodules of mutants SGEFix$^-$-2 (*sym33*), SGEFix$^-$-3 (*sym26*) and SGEFix$^-$-1 (*sym40*) is difficult to explain, but a common sharp decrease in abundance in 28-day-old nodules may indicate the activation of early senescence in nodules of these mutants (Serova et al. 2018). Thus, we suggest that membrane-anchored AGP may be a marker of symbiosome maturation and/or it may play a role in the symbiosome differentiation.

In summary, the present study has analysed the tissue distribution and subcellular localisation of pectins and arabinogalactan proteins (AGPs) in wild-type and ineffective nodules of *P. sativum* and *M. truncatula*. The highly methylesterified homogalacturonan (HG) detected by monoclonal antibody JIM7 showed a uniform localisation in the cell wall, regardless of the cell type in nodules of both species. On the other hand, low methylesterified HG recognised by JIM5 was detected mainly in the walls of infection threads. The differences in localisation of RG-I and membrane-anchored AGP between wild-type lines, as well as between mutant lines in orthologous genes in *P. sativum* and *M. truncatula*, indicate that slightly different cell wall components are present at the plant–microbe interface in different situations.

The development of the nodule, and especially the growth of the infection thread and the differentiation of the symbiosome, involves close coupling at the plant–microbe interface leading to cell wall remodelling and reorganisation of the underlying architecture of the cytoskeleton (Kitaeva et al. 2016). Future comparative analysis will help to identify the components of these processes that are unique to cell surface interactions during symbiosis and the components that play a more general role in the cell biology of legumes.

**Acknowledgements** We thank Jean-Marie Prosperi (INRA, Montpellier, France) for providing *M. truncatula* seeds, Peter Mergaert (Institut des Sciences Végétal, Gif sur Yvette, France) for the kind gift of seeds of the *M. truncatula dnf1–1* mutant line and Pascal Gamas (Laboratoire des Interactions Plantes-Microorganismes, Castanet-Tolosan, France) for the kind gift of seeds TR3 and *efd–1* mutants. The research was performed using equipment of the Core Centrum "Genomic Technologies, Proteomics and Cell Biology" in ARRIAM and the "Molecular and Cell Technologies" Research Resource Centre at Saint-Petersburg State University.

**Funding information** This work was financially supported by Russian Science Foundation (16–16–10035).



## References

Andersen MCF, Boos I, Marcus SE, Kračun SK, Rydahl MG, Willats WGT, Knox JP, Clausen MH (2016) Characterization of the LM5 pectic galactan epitope with synthetic analogues of β-1,4-D-galactotetraose. Carbohydr Res 436:36–40

Anderson CT (2015) We be jammin': an update on pectin biosynthesis, trafficking and dynamics. J Exp Bot 67:495–502

Balestrini R, Hahn MG, Faccio A, Mendgen K, Bonfante P (1996) Differential localization of carbohydrate epitopes in plant cell walls in the presence and absence of arbuscular mycorrhizal fungi. Plant Physiol 111:203–213

Bellincampi D, Cervone F, Lionetti V (2014) Plant cell wall dynamics and wall-related susceptibility in plant–pathogen interactions. Front Plant Sci 5:228

Borisov AY, Rozov S, Tsyganov V, Kulikova O, Kolycheva A, Yakobi L, Ovtsyna A, Tikhonovich I (1994) Identification of symbiotic genes in pea (*Pisum sativum* L.) by means of experimental mutagenesis. Genetika (Russian Federation) 30:1484–1494

Borisov AY, Rozov SM, Tsyganov VE, Morzhina EV, Lebsky VK, Tikhonovich IA (1997) Sequential functioning of *Sym-13* and *Sym-31*, two genes affecting symbiosome development in root nodules of pea (*Pisum sativum* L). Mol Gen Genet 254:592–598

Bradley DJ, Wood EA, Larkins AP, Galfre G, Butcher GW, Brewin NJ (1988) Isolation of monoclonal antibodies reacting with

peribacteriod membranes and other components of pea root nodules containing *Rhizobium leguminosarum*. Planta 173:149–160
Brewin NJ (2004) Plant cell wall remodelling in the Rhizobium–legume symbiosis. Crit Rev Plant Sci 23:293–316
Caffall KH, Mohnen D (2009) The structure, function, and biosynthesis of plant cell wall pectic polysaccharides. Carbohydr Res 344:1879–1900
Cheng H-P, Walker GC (1998) Succinoglycan is required for initiation and elongation of infection threads during nodulation of alfalfa by *Rhizobium meliloti*. J Bacteriol 180:5183–5191
Corral-Martínez P, García-Fortea E, Bernard S, Driouich A, Seguí-Simarro JM (2016) Ultrastructural immunolocalization of arabinogalactan protein, pectin and hemicellulose epitopes through anther development in *Brassica napus*. Plant Cell Physiol 57:2161–2174
Cosgrove DJ (2005) Growth of the plant cell wall. Nat Rev Mol Cell Biol 6:850–861
Dahiya P, Sherrier DJ, Kardailsky IV, Borisov AY, Brewin NJ (1998) Symbiotic gene *Sym31* controls the presence of a lectinlike glycoprotein in the symbiosome compartment of nitrogen-fixing pea nodules. Mol Plant-Microbe Interact 11:915–923
Ellis M, Egelund J, Schultz CJ, Bacic A (2010) Arabinogalactan-proteins (AGPs): key regulators at the cell surface? Plant Physiol 153:403–419
Fåhraeus G (1957) The infection of clover root hairs by nodule bacteria studied by a simple glass slide technique. J Gen Microbiol 16:374–381
Gavrin A, Chiasson D, Ovchinnikova E, Kaiser BN, Bisseling T, Fedorova EE (2016) VAMP721a and VAMP721d are important for pectin dynamics and release of bacteria in soybean nodules. New Phytol 210:1011–1021
Gawecki R, Sala K, Kurczyńska EU, Świątek P, Płachno BJ (2017) Immunodetection of some pectic, arabinogalactan proteins and hemicellulose epitopes in the micropylar transmitting tissue of apomictic dandelions (Taraxacum, Asteraceae, Lactuceae). Protoplasma 254:657–668
Gorshkova T, Kozlova L, Mikshina P (2013) Spatial structure of plant cell wall polysaccharides and its functional significance. Biochem Mosc 78:836–853
Herbette S, Bouchet B, Brunel N, Bonnin E, Cochard H, Guillon F (2014) Immunolabelling of intervessel pits for polysaccharides and lignin helps in understanding their hydraulic properties in *Populus tremula×alba*. Ann Bot 115:187–199
Ivanova KA, Tsyganova AV, Brewin NJ, Tikhonovich IA, Tsyganov VE (2015) Induction of host defences by *Rhizobium* during ineffective nodulation of pea (*Pisum sativum* L.) carrying symbiotically defective mutations *sym40* (*PsEFD*), *sym33* (*PsIPD3/PsCYCLOPS*) and *sym42*. Protoplasma 252:1505–1517
Jones L, Seymour GB, Knox JP (1997) Localization of pectic galactan in tomato cell walls using a monoclonal antibody specific to (1→4)-$\beta$-D-Galactan. Plant Physiol 113:1405–1412
Kardailsky IV, Sherrier DJ, Brewin NJ (1996) Identification of a new pea gene, *PsNlec1*, encoding a lectin-like glycoprotein isolated from the symbiosomes of root nodules. Plant Physiol 111:49–60
Kitaeva AB, Demchenko KN, Tikhonovich IA, Timmers ACJ, Tsyganov VE (2016) Comparative analysis of the tubulin cytoskeleton organization in nodules of *Medicago truncatula* and *Pisum sativum*: bacterial release and bacteroid positioning correlate with characteristic microtubule rearrangements. New Phytol 210:168–183
Knox JP (2008) Revealing the structural and functional diversity of plant cell walls. Curr Opin Plant Biol 11:308–313
Knox JP, Roberts K (1989) Carbohydrate antigens and lectin receptors of the plasma membrane of carrot cells. Protoplasma 152:123–129
Knox JP, Linstead PJ, King J, Cooper C, Roberts K (1990) Pectin esterification is spatially regulated both within cell walls and between developing tissues of root apices. Planta 181:512–521
Kosterin OE, Rozov SM (1993) Mapping of the new mutation *blb* and the problem of integrity of linkage group I. Pisum Genet 25:27–31
Levesque-Tremblay G, Pelloux J, Braybrook SA, Müller K (2015) Tuning of pectin methylesterification: consequences for cell wall biomechanics and development. Planta 242:791–811
Lionetti V, Cervone F, Bellincampi D (2012) Methyl esterification of pectin plays a role during plant–pathogen interactions and affects plant resistance to diseases. J Plant Physiol 169:1623–1630
Liu J, Hou J, Chen H, Pei K, Li Y, He X-Q (2017) Dynamic changes of pectin epitopes in cell walls during the development of the procambium–cambium continuum in poplar. Int J Mol Sci 18:1716
Maunoury N, Redondo-Nieto M, Bourcy M, Van de Velde W, Alunni B, Laporte P, Durand P, Agier N, Marisa L, Vaubert D, Delacroix H, Duc G, Ratet P, Aggerbeck L, Kondorosi E, Mergaert P (2010) Differentiation of symbiotic cells and endosymbionts in *Medicago truncatula* nodulation are coupled to two transcriptome-switches. PLoS One 5:e9519
Nemankin N (2011) Analysis of pea (*Pisum sativum* L.) genetic system, controlling development of arbuscular mycorrhiza and nitrogen-fixing symbiosis. Dissertation Saint-Petersburg State University (in Russian)
Nguema-Ona E, Vicré-Gibouin M, Cannesan M-A, Driouich A (2013) Arabinogalactan proteins in root–microbe interactions. Trends Plant Sci 18:440–449
Ovchinnikova E, Journet E-P, Chabaud M, Cosson V, Ratet P, Duc G, Fedorova E, Liu W, den Camp RO, Zhukov V, Tikhonovich I, Borisov A, Bisseling T, Limpens E (2011) IPD3 controls the formation of nitrogen-fixing symbiosomes in pea and *Medicago* Spp. Mol Plant-Microbe Interact 24:1333–1344
Perotto S, Vandenbosch KA, Butcher GW, Brewin NJ (1991) Molecular composition and development of the plant glycocalyx associated with the Peribacteroid membrane of pea root-nodules. Development 112:763–773
Rae AL, Bonfante-Fasolo P, Brewin NJ (1992) Structure and growth of infection threads in the legume symbiosis with *Rhizobium leguminosarum*. Plant J 2:385–395
Rich MK, Schorderet M, Reinhardt D (2014) The role of the cell wall compartment in mutualistic symbioses of plants. Front Plant Sci 5:238
Ruprecht C, Bartetzko MP, Senf D, Dallabernardina P, Boos I, Andersen MC, Kotake T, Knox JP, Hahn MG, Clausen MH (2017) A synthetic glycan microarray enables epitope mapping of plant cell wall glycan-directed antibodies. Plant Physiol 175:1094–1104
Rydahl MG, Hansen AR, Kračun SK, Mravec J (2018) Report on the current inventory of the toolbox for plant cell wall analysis: proteinaceous and small molecular probes. Front Plant Sci 9:581
Saffer AM (2018) Expanding roles for pectins in plant development. J Integr Plant Biol 60:910–923
Sala K, Malarz K, Barlow PW, Kurczyńska EU (2017) Distribution of some pectic and arabinogalactan protein epitopes during *Solanum lycopersicum* (L.) adventitious root development. BMC Plant Biol 17:25
Serova TA, Tsyganova AV, Tsyganov VE (2018) Early nodule senescence is activated in symbiotic mutants of pea (*Pisum sativum* L.) forming ineffective nodules blocked at different nodule developmental stages. Protoplasma 255:1443–1459
Sherrier DJ, Borisov AY, Tikhonovich IA, Brewin NJ (1997) Immunocytological evidence for abnormal symbiosome development in nodules of the pea mutant line Sprint-2Fix$^-$ (*sym31*). Protoplasma 199:57–68
Sherrier DJ, Prime TA, Dupree P (1999) Glycosylphosphatidylinositol-anchored cell-surface proteins from *Arabidopsis*. Electrophoresis 20:2027–2035
Showalter AM (2001) Arabinogalactan-proteins: structure, expression and function. Cell Mol Life Sci 58:1399–1417

Sujkowska-Rybkowska M, Borucki W (2015) Pectins esterification in the apoplast of aluminum-treated pea root nodules. J Plant Physiol 184: 1–7

Torode TA, O'Neill R, Marcus SE, Cornuault V, Pose S, Lauder RP, Kračun SK, Rydahl MG, Andersen MC, Willats WG (2018) Branched pectic galactan in phloem-sieve-element cell walls: implications for cell mechanics. Plant Physiol 176:1547–1558

Tsyganov VE, Borisov AY, Rozov SM, Tikhonovich IA (1994) New symbiotic mutants of pea obtained after mutagenesis of laboratory line SGE. Pisum Genet 26:36–37

Tsyganov VE, Morzhina EV, Stefanov SY, Borisov AY, Lebsky VK, Tikhonovich IA (1998) The pea (*Pisum sativum* L.) genes *sym33* and *sym40* control infection thread formation and root nodule function. Mol Gen Genet 259:491–503

Tsyganov VE, Voroshilova VA, Borisov AY, Tikhonovich IA, Rozov SM (2000) Four more symbiotic mutants obtained using EMS mutagenesis of line SGE. Pisum Genet 32:63

Tsyganova AV, Tsyganov V, Borisov AY, Tikhonovich IA, Brewin NJ (2009a) Comparative cytochemical analysis of hydrogen peroxide distribution in pea ineffective mutant SGEFix$^{-}$-1 *(sym40)* and initial line SGE. Ecol Genet 7(3):3–9

Tsyganova AV, Tsyganov VE, Findlay KC, Borisov AY, Tikhonovich IA, Brewin NG (2009b) Distribution of legume arabinogalactanprotein-extensin (AGPE) glycoproteins in symbiotically defective pea mutants with abnormal infection threads. Cell Tissue Biol 51:53–62

Van de Velde W, Zehirov G, Szatmari A, Debreczeny M, Ishihara H, Kevei Z, Farkas A, Mikulass K, Nagy A, Tiricz H, Satiat-Jeunemaître B, Alunni B, Bourge M, Kucho K-I, Abe M, Kereszt A, Maroti G, Uchiumi T, Kondorosi E, Mergaert P (2010) Plant peptides govern terminal differentiation of bacteria in symbiosis. Science 327:1122–1126

Verhertbruggen Y, Marcus SE, Haeger A, Ordaz-Ortiz JJ, Knox JP (2009) An extended set of monoclonal antibodies to pectic homogalacturonan. Carbohydr Res 344:1858–1862

Vernié T, Moreau S, de Billy F, Plet J, Combier J-P, Rogers C, Oldroyd G, Frugier F, Niebel A, Gamas P (2008) EFD is an ERF transcription factor involved in the control of nodule number and differentiation in *Medicago truncatula*. Plant Cell 20:2696–2713

Voroshilova VA, Boesten B, Tsyganov VE, Borisov AY, Tikhonovich IA, Priefer UB (2001) Effect of mutations in *Pisum sativum* L. genes blocking different stages of nodule development on the expression of late symbiotic genes in *Rhizobium leguminosarum* bv. *viciae*. Mol Plant-Microbe Interact 14:471–476

Wang TL, Wood EA, Brewin NJ (1982) Growth regulators, *Rhizobium* and nodulation in peas. Planta 155:350–355

Wang D, Griffitts J, Starker C, Fedorova E, Limpens E, Ivanov S, Bisseling T, Long S (2010) A nodule-specific protein secretory pathway required for nitrogen-fixing symbiosis. Science 327:1126–1129

Willats WG, Steele-King CG, Marcus SE, Knox JP (1999) Side chains of pectic polysaccharides are regulated in relation to cell proliferation and cell differentiation. Plant J 20:619–628